Biosensors and Bioelectronics 64 (2015) 579–585

Contents lists available at ScienceDirect

Biosensors and Bioelectronics

journal homepage: www.elsevier.com/locate/bios

A controlled microfluidic electrochemical lab-on-a-chip for label-free diffusion-restricted DNA hybridization analysis

Hadar Ben-Yoav [a,*,1], Peter H. Dykstra [a,1], William E. Bentley [b], Reza Ghodssi [a,b,*]

[a] MEMS Sensors and Actuators Laboratory (MSAL), Department of Electrical and Computer Engineering, Institute for Systems Research, University of Maryland, College Park, MD 20742, USA
[b] Fischell Department of Bioengineering, University of Maryland, College Park, MD 20742, USA

ARTICLE INFO

Article history:
Received 1 July 2014
Received in revised form
22 September 2014
Accepted 24 September 2014

Keywords:
DNA hybridization sensing
Microfluidics
Valve
Label-free detection
Electrochemical impedance spectroscopy
Restricted diffusion

ABSTRACT

Lab-on-a-chip (LOC) devices for electrochemical analysis of DNA hybridization events offer a technology for real-time and label-free assessment of biomarkers at the point-of-care. Here, we present a microfluidic LOC, with 3×3 arrayed electrochemical sensors for the analysis of DNA hybridization events. A new dual layer microfluidic valved manipulation system is integrated providing controlled and automated capabilities for high throughput analysis. This feature improves the repeatability, accuracy, and overall sensing performance (Fig. 1). The electrochemical activity of the fabricated microfluidic device is validated and demonstrated repeatable and reversible Nernstian characteristics. System design required detailed analysis of energy storage and dissipation as our sensing modeling involves diffusion-related electrochemical impedance spectroscopy. The effect of DNA hybridization on the calculated charge transfer resistance and the diffusional resistance components is evaluated. We demonstrate a specific device with an average cross-reactivity value of 27.5%. The device yields semilogarithmic dose response and enables a theoretical detection limit of 1 nM of complementary ssDNA target. This limit is lower than our previously reported non-valved device by 74% due to on-chip valve integration providing controlled and accurate assay capabilities.

1. Introduction

Microfluidic lab-on-a-chip (LOC) devices provide numerous advantages in clinical diagnostics, environmental monitoring and biomedical research. These devices utilize microfluidic channels to control fluid flow throughout the chip, in which a variety of procedures can be arranged side-by-side, including reagent mixing, affinity based binding, signal transduction and cell culturing (Hong et al., 2009; Sun and Kwok, 2006; Xu et al., 2010; Yang and Woolley, 2010). Microfluidics provides many advantages over conventional clinical diagnostic tools. Microfluidic devices require 2–3 orders of magnitude less reagents in comparison to microwell plate readers or electrophoretic gel shift assays when used for similar tasks. These devices can also increase the speed of some biological events due to the smaller confinement of species within the channels (Gervais and Jensen, 2006; Song and Ismagilov, 2003). Thirdly, sensors can be integrated within microfluidic devices to enable label-free detection. Lastly, these devices are inexpensive to produce and often require minimal operator time and skill (Craighead, 2006; Dittrich and Manz, 2006; Dutse and Yusof, 2011; Jiang et al., 2011).

DNA hybridization detection is used extensively to diagnose genetic disorders (Chee et al., 1996; Ma et al., 2006) and various forms of cancer (Ito et al., 2007). For example, it is estimated that approximately 235,000 people will be diagnosed for breast cancer using DNA hybridization measurements in 2014 alone (Siegel et al., 2014). There is a tremendous need for a bench-top microfluidic device that can perform the same assay techniques as a plate reader or gel shift assay at a fraction of the cost and the time to test without sacrificing sensitivity or specificity. Using electrochemical sensors to perform biological and chemical detection in microfluidic systems is very advantageous. The fabrication is inherently less complicated since these sensors typically only require patterned electrodes to operate. In addition, electrochemical signals can be directly interfaced with most measurement equipment while other signal modalities may require a transducer to convert the signal (Dukkipati and Pang, 2006; Fang et al., 2009; Pavlovic et al., 2008; Xu et al., 2009). Additional advances have appeared using microfluidics for DNA hybridization (Henry and O'

* Correspondence to: Institute for Systems Research, Department of Electrical and Computer Engineering, University of Maryland, College Park, MD 20742, USA. Fax: +1 301 314 9920.
E-mail addresses: benyoav@umd.edu (H. Ben-Yoav), ghodssi@umd.edu (R. Ghodssi).
[1] These authors contributed equally to this paper.

http://dx.doi.org/10.1016/j.bios.2014.09.069
0956-5663/

Sullivan, 2012; Kim et al., 2006; Tai et al., 2013; Xu et al., 2009; Yang et al., 2014) although limitations have likely hampered progress. The most important limitations to overcome include: sample preparation and mixing of fluids (due to the low sample volume and low Reynolds number), physical and chemical effects (including capillary forces, surface roughness, chemical interactions between construction materials and analytes), and low electrochemical signal-to-noise ratio (produced by the reduced surface area and volume) (Beebe et al., 2002; Bhushan, 2010; Ghallab and Badawy, 2010; Mariella, 2008). These limitations cause decreased probe surface density, changing their orientation, presence of interfering oligonucleotides leading to potential mismatches, and restricted diffusion and mass transport of target oligonucleotides under static conditions towards surface hybridization (Henry and O'Sullivan, 2012). Overcoming these limitations could accelerate miniaturized device's development with the many advantages into clinical environments.

In this work, we present a microfluidic electrochemical LOC, with an array of individually addressable reaction chambers for the analysis of DNA hybridization. The device is fabricated using polymeric and thin film fabrication technology and is integrated with a microfluidic valved manipulation system. This manipulation system provides programmable and automated capability for high throughput analysis, improving the overall accuracy and performance (Fig. 1). The electrochemical performance of the device was initially characterized using a conventional redox couple (ferrocyanide/ferricyanide). Then the device was tested for detecting and analyzing DNA hybridization. Single stranded DNA (ssDNA, 30-mers) probes were functionalized onto patterned gold electrodes. Electrochemical impedance spectroscopy (EIS) was used to detect hybridization between the ssDNA probe and its complementary ssDNA target. Biosensing performance was evaluated by applying a restricted diffusion-based electrical model (Ben-Yoav et al., 2012, 2011; Bisquert and Compte, 2001) to analyze the EIS measurements. The analysis results allowed to evaluate charge transfer and diffusion resistance yielding accurate determination of DNA hybridization. Our system is capable of theoretically detecting hybridization at 1 nM.

2. Materials and methods

2.1. LOC design and fabrication

The electrode layout is designed to provide individually addressable working electrodes in an array (Fig. 2A). The design used in this work contains nine sensors patterned in a 3×3 grid, modified from Dykstra et al. (2011), and microfabricated on borosilicate glass wafers (Promptar, CA). The counter and the working electrodes (each working electrode is a disk of 100 μm radius) are made of gold, while the reference electrode is made of platinum. A gold working electrode has been chosen due to the gold–sulfur bond that is formed between the thiol groups of the self-assembled probe ssDNA and itself, and platinum has been chosen as the reference electrode material due to its stable reference potential (Pavlovic et al., 2008).

The microfluidic valved chip is comprised of two layers of microchannels made of polydimethylsiloxane (PDMS); a bottom layer with assay channels and a top layer with valves (Fig. 2B illustrates layouts of the top and the bottom channels). The bottom microfluidic assay channels (32 μm in height and 500 μm in width) are formed by spinning a 20:1 ratio of PDMS (1000 RPM; 55 μm thick) over a patterned AZ 9260 photoresist mold ("assay mold"). Prior to PDMS spinning, the photoresist mold is heated, rounding its profile, and trimethylchlorosilane (Gelest, PA) is evaporated under vacuum conditions. This chemical agent covers the surface of the mold, a step that will ease the subsequent thin film PDMS release. The curing of the PDMS with the assay channels is performed in an oven at 80 °C for 17 min. Then the top valve channels (100 μm in height and 300 μm in width) are fabricated through casting of a 5:1 ratio of PDMS over another differently patterned SU-8 photoresist mold ("valve mold"). The curing of the PDMS with the valve channels is performed in an oven at 80 °C for 17 min. After carefully cutting a piece from the top valve channels PDMS and aligning over the spun assay channels PDMS, the dual-layer PDMS is cured in an oven at 80 °C for 3 h, to promote stronger bond between the two layers since they each contain a different ratio of curing agent.

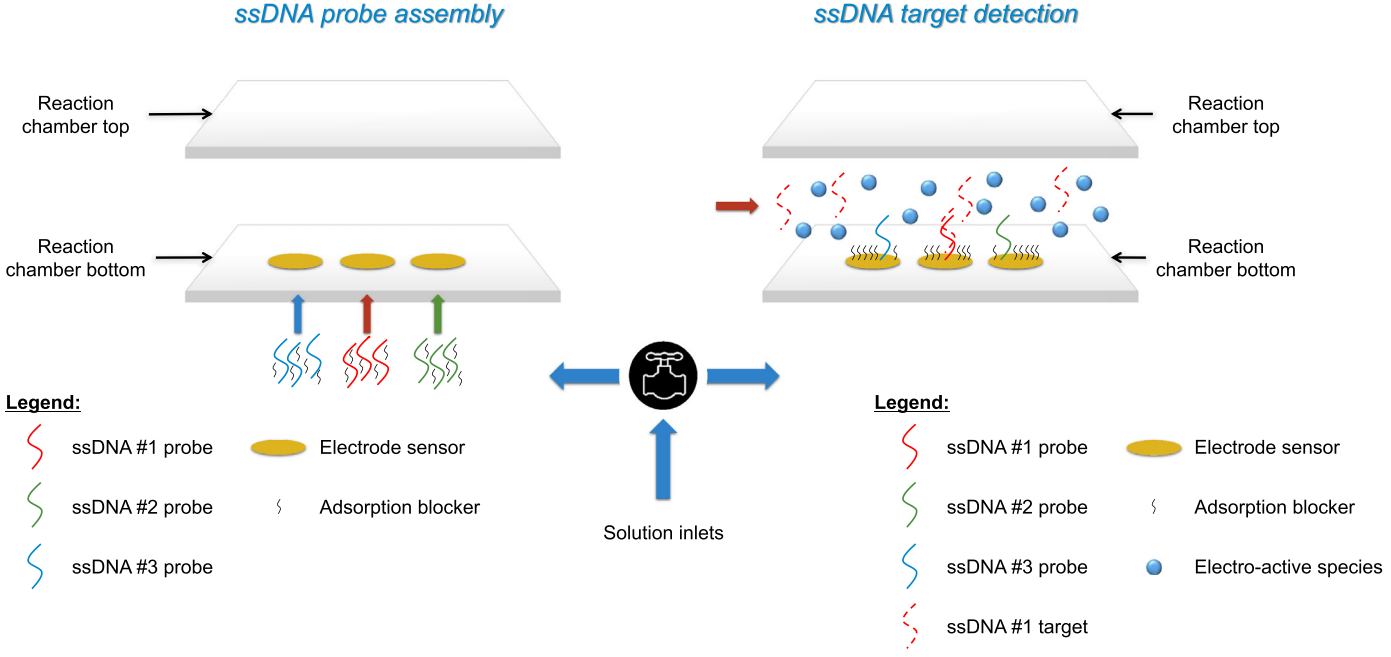

Fig. 1. Valved-based controlled lab-on-a-chip for improved DNA hybridization detection. Left: ssDNA probe assembly. Right: ssDNA target detection due to DNA hybridization event.

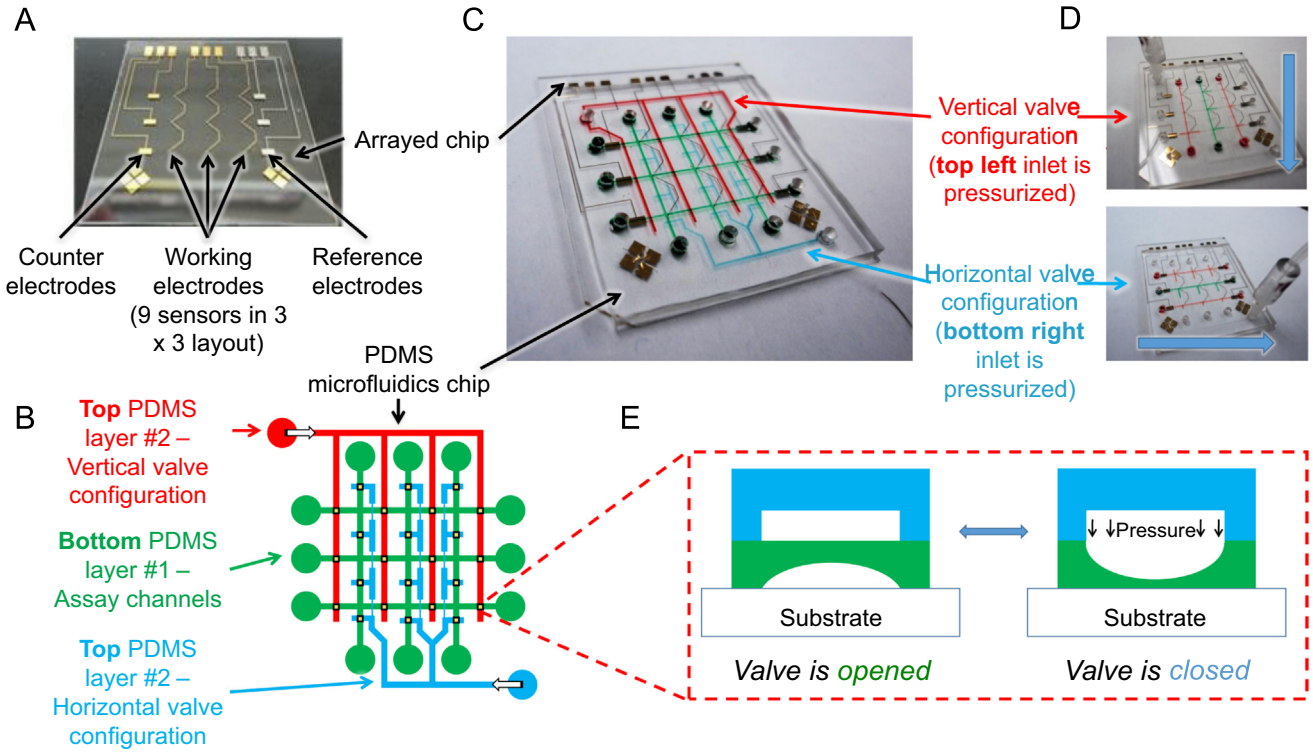

Fig. 2. Microfluidic valved arrayed electrochemical LOC. (A) Photographs of the fabricated arrayed electrochemical chip (3.5 cm × 4 cm). (B) Layout of the top valve configuration (blue or red) and the bottom assay (green) channels. (C) A photograph of the entire assembled device. Assay channels are filled with green dye, and valve channels are filled with either blue or red dye for horizontal or vertical assay channels orientation, respectively. (D) Photographs of the vertical (top) and the horizontal (bottom) valve configurations with the resulted assay channels orientation filled with red and green dyes. Thick arrows indicate fluid flow direction. (E) Schematic demonstrating valve actuation using hydraulic channel to pinch off the microfluidic assay channel below. Left – valve is opened when no pressure is applied. Right – valve is closed upon pressure application.

After peeling the dual-layer PDMS away from the mold, twelve fluid inlets and outlets of 1 mm radius are punched through the PDMS. The PDMS chip and the patterned electrodes chip are bonded by exposing both chips to oxygen plasma followed by adding a drop of methanol and aligning by eye such that each electrode in a row or column lies in its own separate reaction chamber. An irreversible bond forms between the PDMS and glass surface, which provides a leak-proof seal during the experiments. Micropositioning probes are used for electrical contact to pads on the outer edge of the chip. The completed device is shown in Fig. 2C.

Hydraulic valve operation is achieved using pressurized air (5 psi) either applied to the top left or bottom right inlet to form vertical or horizontal microfluidic assay channels passing over the sensor array (Fig. 2D). The valve channels are filled with water prior to pressure application to prevent air bubbles from leaking through the PDMS and into the channel. The increase in pressure causes the PDMS membrane to bend downward closing the valve and sectioning the bottom assay channel (Fig. 2E), while releasing the pressure causes the valve to open. The assay channels are filled with the sample solutions at a flow rate of 30 μL/h using a syringe pump (Kent Scientific, CT).

The electrodes are arranged in a grid format to expose either rows or columns of electrodes, dependent on the microfluidic valved chip configuration. A vertical configuration results in three columns of three working electrodes each that can be functionalized with three different probes. A horizontal configuration results in a three-electrode system of three sensors (each working electrode sensor is spaced 5 mm apart), a counter electrode, and a reference electrode. These programmable vertical and horizontal configurations allow functionalization of multiple sensor surfaces with specific probes without cross-contamination, followed by parallel incubation and testing with multiple samples.

2.2. DNA, solutions and instruments

ssDNA sequences were purchased from Integrated DNA Technologies (Coralville, IA). All chemicals were purchased from Sigma-Aldrich (St. Louis, MO). The buffers for all experiments was either 10 mM phosphate buffer solution (PBS) with 100 mM NaCl or 4x saline sodium citrate (SSC). Three probe sequences and two complementary target sequences were chosen as a model system for complementary and non-complementary DNA hybridization events (for ssDNA sequences refer to Table S1), were each re-suspended in a buffer solution containing 10 mM Tris, 50 mM NaCl and 1 mM EDTA and frozen at −20 °C in 20 μL aliquots until further use. Prior to electrode functionalization the probes were diluted to a 1 μM concentration with 10 mM PBS, 100 mM NaCl, and 10 μM Tris (2-carboxyethyl) phosphine (TCEP). A probe concentration of 1 μM was chosen based on studies performed by other groups demonstrating a high surface density of molecules (approximately 3×10^{12} molecules/cm^2; Ricci et al., 2007). 1 mM 6-mercapto-1-hexanol (MCH) passivation solution was prepared in 10 mM PBS. Incubation solution with the target sequence was prepared in 4x SSC buffer. All electrochemical tests were performed with a CHI660D single channel potentiostat from CH Instruments (Austin, TX). The electrolyte used in all impedance experiments was 10 mM PBS with 100 mM NaCl along with 10 mM ferricyanide and 10 mM ferrocyanide yielding a solution with the reversible redox couple $[Fe(CN)_6]^{4-}/[Fe(CN)_6]^{3-}$ ions.

2.3. Microfluidic valved LOC electrochemical characterization assays

The microfluidic valved LOC is evaluated by testing its electrochemical performance for the analysis of a known electrochemical reaction. Therefore, the reversible redox couple ferrocyanide/ferricyanide is used as a model system to characterize the Nernstian electrochemical response of the device. This assay is evaluated by conventional cyclic voltammetry (CV) technique at 25, 50, 100, 150, 200, and 250 mV/s scan rates.

2.4. Microfluidic valved LOC DNA hybridization tests

Surface preparation followed by electrochemical activity validation of every working electrode is done prior to the DNA hybridization experiments by testing ferrocyanide/ferricyanide redox couple solution using the CV method with multiple cycles. Then, a vertical channel configuration is applied, and the electrodes are functionalized using a solution containing 1 μM probe ssDNA for 3 h followed by a PBS rinse step. Each vertical channel is functionalized with a different probe. For dose response tests the duration of the probe functionalization is extended to overnight (~18 h) to provide higher hybridization signals due to higher probe densities (Ricci et al., 2007). The electrodes are incubated overnight (~18 h) in a solution of 1 mM MCH to passivate any exposed regions on the surface of the electrode to reduce non-specific binding effects (McEwen et al., 2009). Incubation with the target sequence is performed in the horizontal channel configuration with 0.01, 0.1, 1, and 10 μM of the complementary target DNA and 1 μM of the non-complementary target DNA for 20 min. EIS measurements are performed in the presence of the ferrocyanide/ferricyanide redox couple solution, in a range of frequencies between 0.1 MHz and 1 Hz (12 frequency data points per frequency decade, 25 mV amplitude) while the working electrode is left at open circuit potential vs. the platinum reference electrode. All impedance spectroscopy experiments are performed in triplicate and equivalent electrical circuit fitting is done using EC-Lab software (v10.33, Bio-Logic SAS, France).

3. Results and discussion

3.1. Electrochemical characterization of the microfluidic valved LOC

The microfluidic valved LOC has the capability to measure electrochemical reactions on nine different working electrodes. The electrochemical activity of the device was characterized with the redox couple ferrocyanide/ferricyanide filling the assay microchannels. Fig. 3 shows CVs of all nine working electrodes in the device. The CVs demonstrated reversible Nernstian characteristics for all electrodes. A small variation with the amplitude of the current between horizontal channels was observed (anodic current peak comparison: bottom channel was 0.55 ± 0.05 μA; middle channel was 0.95 ± 0.02 μA; top channel was 0.80 ± 0.03 μA). This variation is because of fabrication challenges and misalignment issues. Misalignment between the PDMS assay channels and the working electrodes on the electrochemical chip causes the channels to partially expose the electrodes to the solution, revealing uneven surface areas. These unevenly exposed electrodes generate variable electrochemical current among channels.

Fig. 4A presents increasing overall CV current values for increasing scan rates. The peak of the anodic and the cathodic currents and the associated applied potential (vs. platinum open reference electrode) were extracted and plotted versus the square root of the scan rate and the scan rate of the CV, respectively (Fig. 4B and C). The current peak plot (Fig. 4B) yielded linear relationships with slope values of $3.50 \times 10^{-6} \pm 0.06 \times 10^{-6}$ A*(s/V)^2 and $-3.75 \times 10^{-6} \pm 0.02 \times 10^{-6}$ A*(s/V)^2 corresponding to the anodic and the cathodic currents. These values are very close to the expected relation of 2.6×10^{-6} A*(s/V)^2 and -2.4×10^{-6}A*(s/V)^2, respectively, calculated by Bard and Faulkner (2001) (Konopka and McDuffie, 1970). Furthermore, a linear relationship was observed between the applied potential at the anodic and the cathodic peaks and the scan rate of CV (Fig. 4C). This dependence may be attributed to the fact that the Nernst equation is slightly modified on very small electrodes, where current flow causes an increase in the ohmic drop (uncompensated resistance and solution resistance) near the electrode (Andrieux et al., 1990; Nicholson, 1965). Another reason for such dependence may be due to the change of the electro-active species concentration next to the electrode during relatively extreme (slow and fast) scan rates that cause the standard reduction potential to change (Bard and Faulkner, 2001).

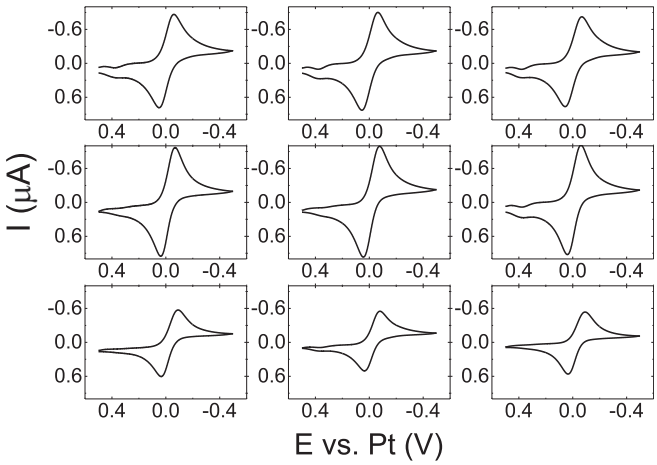

Fig. 3. Electrochemical validation of the LOC. CV scans with ferrocyanide/ferricyanide solution for each of the nine working electrode sensors in the microfluidic valved LOC. The CVs are arranged in the same 3×3 grid as the physical sensor layout.

3.2. Microfluidic valved LOC for DNA hybridization analysis

The biosensing performance of the LOC was tested with different ssDNA probes and targets. Initially, EIS measurements of the device modified with an ssDNA probe were recorded in the presence of a redox couple (ferrocyanide/ferricyanide) following an incubation step with a complementary and a non-complementary ssDNA targets (Fig. 5A). Results indicate higher impedance values after incubation with a non-complementary ssDNA target as opposed to a complementary ssDNA. In addition, these impedance values are higher than those measured by a bare electrode without probe functionalization. Such characteristics suggest that functionalizing the electrode surface with the ssDNA probe increases the charge transfer resistance. The charge transfer resistance increase could be attributed to the increased repulsion forces between the negatively charge redox couple and the negatively charged ssDNA probe molecules functionalizing the surface of the electrode. The observation that introducing a complementary ssDNA resulted in lower impedance values than a non-complementary ssDNA suggests that the charge transfer resistance decreases upon DNA hybridization event. The ssDNA probes are lying flat against the MCH layer before introducing the matching target. Upon hybridization, the rigidity of the double helix structure causes the probes to release from the substrate and stand upright. This change in the DNA orientation can create more ion paths for the redox compound to approach the electrode surface and consequently result in a reduction of the measured

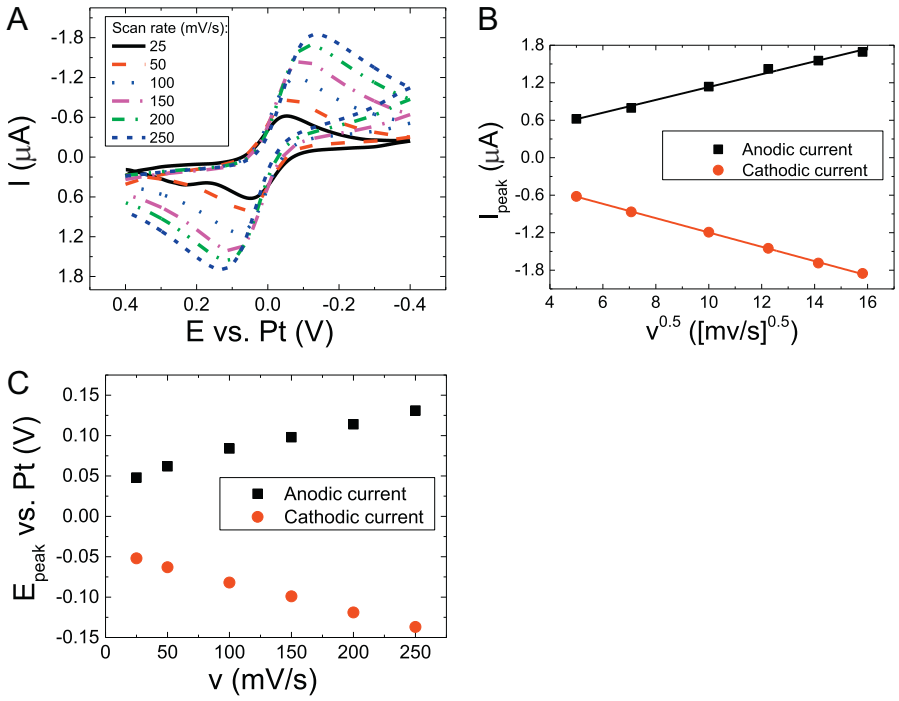

Fig. 4. Electrochemical characterization of the LOC. (A) CV scans at 25, 50, 100, 150, 200, and 250 mV/s scan rates of an electrode in the microfluidic valved system. (B) The influence of the square root of the scan rate on either the anodic (black squares) or the cathodic (red circles) peak currents. (C) The effect of the scan rate on the potential at either the anodic (black squares) or the cathodic (red circles) peak current.

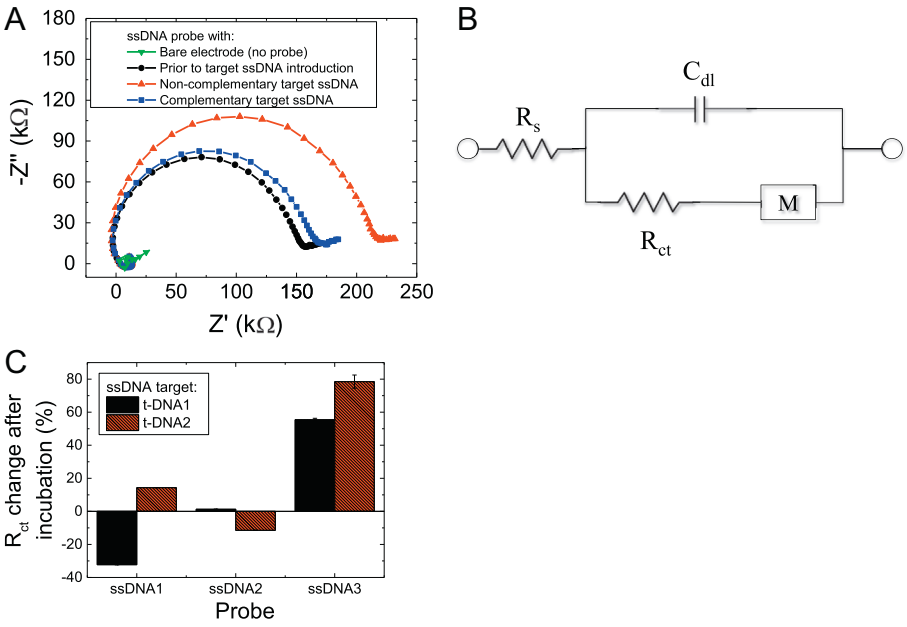

Fig. 5. (A) Nyquist plot of impedance spectroscopy measurements of a bare electrode without probe functionalization (green inverted triangles), and an electrode modified with ssDNA probe prior to ssDNA target introduction (black circles) and following incubation with either a complementary (blue squares; 1 μM) or a non-complementary (red triangles; 1 μM) target ssDNA. (B) Diagram of a diffusion-restricted electrical equivalent circuit that was used for impedance spectroscopy analysis. R_s is the solution resistance, R_{ct} is the charge transfer resistance, C_{dl} is the electrode–electrolyte double layer interface, and M is restricted linear ordinary diffusion impedance element with a reflective boundary. (C) The change in percentage of the calculated charge transfer resistance before and after incubation period with two different ssDNA targets for three different ssDNA probes.

impedance (Gooding et al., 2003; Ito et al., 2007; Pan and Rothberg, 2005).

The specificity of the biosensor was tested by evaluating the binding selectivity of two different ssDNA targets with three different complementary ssDNA probes. In order to assess the influence of DNA hybridization events on the electrochemical system, the measured EIS data was fitted to an equivalent electrical circuit presented in Fig. 5B. This model incorporates a diffusion-restricted component with both energy storage and dissipation elements. R_s is the solution resistance, R_{ct} is the charge transfer resistance, C_{dl} is the electrode–electrolyte double layer capacitance, and M is the restricted linear diffusion impedance element with a reflective boundary due to physical and chemical interactions between particles and ions in the electrolyte and the components of the electrochemical system (Ben-Yoav et al., 2012; Bisquert and Compte, 2001). The difference in percentage between

the calculated R_{ct} before and after incubation with either non-complementary or complementary ssDNA targets for three different ssDNA probes is calculated using Eq. (1) and shown in Fig. 5C.

$$R_{ct\ change}(\%) = (R_{ct,after\ \ incubation} - R_{ct,before\ \ incubation}) / R_{ct,before\ \ incubation} \quad (1)$$

The results demonstrated lower $R_{ct\ change}$ values when the complementary ssDNA target was introduced. Furthermore, an averaged cross-reactivity value of 27.5% was calculated in the presence of the non-complementary ssDNA target using Eq. (2).

$$Cross\text{–}reactivity = R_{ct\ change,non-complementary\ \ ssDNA} / R_{ct\ change,complementary\ \ ssDNA} \quad (2)$$

This demonstrates the probe-target specificity with little non-specific binding on the biosensor. The selectivity of the impedance measurements to the presence of the complementary target ssDNA is due to a decrease in the repulsion force between the DNA and the electro-active species (ferrocyanide and ferricyanide) present in the electrolyte (Gooding et al., 2003). The weaker repulsive forces make diffusion easier for electro-active species, reflected by the decrease in the calculated charge transfer resistance (R_{ct}) values.

Different concentrations of complementary ssDNA targets were introduced to the ssDNA probe in order to evaluate the sensitivity of the LOC. Fig. 6A presents a Nyquist plot with EIS measurements for increasing complementary ssDNA target concentrations (0.01, 0.1, 1, and 10 μM). A trend of decreasing low frequency impedance values (~2 Hz) for increasing ssDNA target concentrations was observed. The diffusion-restricted equivalent electrical circuit (Fig. 5B) was fitted to the EIS measurements. Fig. 6B and C presents the influence of the complementary ssDNA target concentration on the calculated charge transfer resistance and the restricted diffusional resistance changes, respectively. The results show a semilogarithmic relationship between the charge transfer resistance and the restricted diffusional resistance at the working electrode and the ssDNA target concentration. Regression analysis of the charge transfer resistance relation resulted in a slope value of $-10.0 \pm 0.7\%$ and an intercept value of $-30.0 \pm 1.2\%$, between the calculated charge transfer resistance change and the ssDNA target concentration (Fig. 6B).

These results demonstrate the ability to quantify DNA hybridization events and analyze their selectivity with the LOC by monitoring charge transfer resistance and restricted diffusional resistance changes in the system. Charge transfer resistance analysis showed a positive relation suggesting that the electrochemical activity of the redox couple is affected by the DNA hybridization events. Increased number of hybridization events can decrease repulsion forces between the DNA and the redox couple, improving their redox reactivity (Gooding et al., 2003). In the case of the positive relationship for the restricted diffusional resistance analysis, we propose that the diffusion of the electroactive species is affected by DNA hybridization. The higher number of hybridization events, which result in weaker repulsion forces between the electrode surface and the complementary ssDNA target, can improve the diffusivity of the redox couple towards the surface (Ben-Yoav et al., 2012; Bisquert and Compte, 2001).

The sensor demonstrated a linear detection range for target ssDNA concentrations lower than 1 μM, and the theoretical limit of detection value was determined to be 1 nM by calculating the corresponding ssDNA target concentration for the background signal with a non-complementary ssDNA (R_{ct} change from non-complementary = 0%). The estimated limit of detection and limit of quantification values were determined to be 28 nM and 64 μM by adding either three or ten standard deviation units to the background signal with a non-complementary ssDNA, respectively (Analytical Methods Committee, 1987). This theoretical limit of detection is better than the previously reported value of 3.8 nM with a non-valved LOC (Ben-Yoav et al., 2012). One main reason for this improvement is the integrated microfluidic valved manipulation system, which provides programmable and automated high

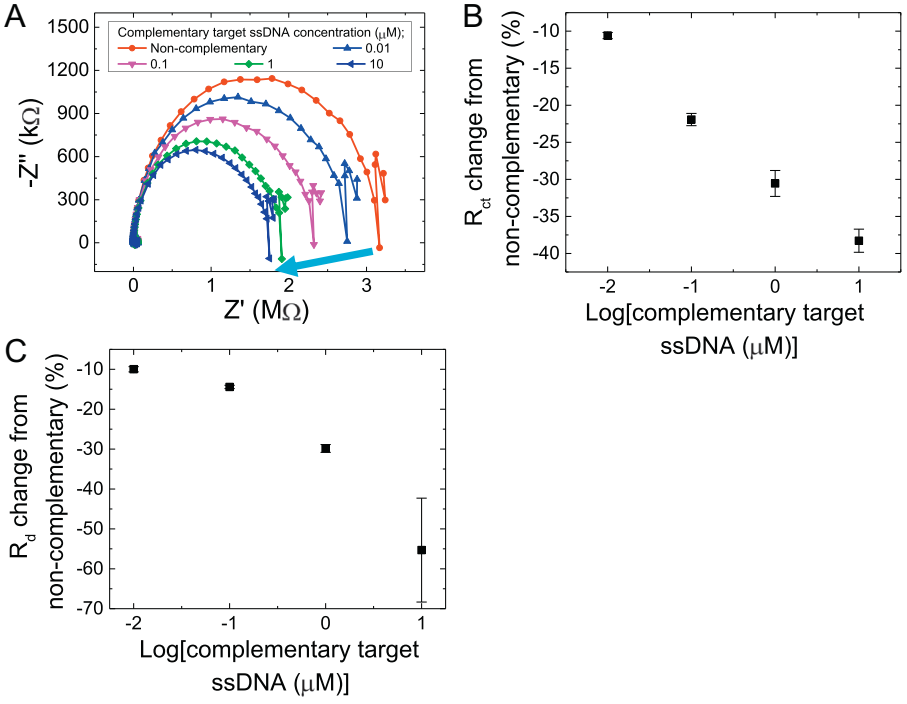

Fig. 6. The influence of the concentration of the complementary ssDNA target on the biosensing mechanism following incubation with 0.01, 0.1, 1, and 10 μM ssDNA target. (A) Nyquist plot of impedance spectroscopy measurements (arrow indicates increasing ssDNA target concentrations; 1 μM non-complementary ssDNA target concentration). The influence of the complementary ssDNA target concentration on the calculated change from non-complementary target ssDNA of (B) charge transfer resistance – R_{ct} (coefficient of variation = 47%) and (C) restricted diffusional resistance – R_d (coefficient of variation = 75%) components.

throughput analysis. These capabilities improve the signal-to-noise ratio and the overall sensing performance of the LOC by increasing experimental control and repeatability and decreasing human factor errors. Another reason is the smaller dimensions of the assay chamber affecting the diffusion layer, hence amplifying the biosensing signal from diffusional reactions. As the biosensing mechanism of DNA hybridization events is dependent on diffusional reactions, the ability to detect these events is enhanced, which improves the overall detection limit.

Different components of the DNA biosensor micro-system affect its sensing performance (i.e., limit of detection and detection range), such as reaction chamber dimensions and geometry, electrode material, ssDNA probe length and density, and electrochemical detection method (Bonanni and del Valle, 2010). For example, integration of nanomaterials as the transducer material can increase the generated electrochemical signal during hybridization events between the probe and the target ssDNA. The choice of the electrochemical detection method can also affect the sensor performance. While faradaic impedance spectroscopy provides higher electrochemical signals that are indirectly related to hybridization events, non-faradaic mode delivers charge variation information that is directly related to DNA configuration and density changes at the surface of the electrode. Through careful consideration of the impact of the micro-system components together with the targeted functionality and application of the device, new sensors with improved accuracy and unique capabilities, such as single nucleotide mismatch analysis and micro-RNA detection can be engineered.

4. Conclusions

This study presents the development and characterization of a microfluidic valved arrayed electrochemical LOC for DNA hybridization analysis. The electrochemical activity of the device is characterized and validated with a redox couple. The specificity and the limit of detection of the biosensor are evaluated using ssDNA probe assembled on the electrode sensor followed by introduction of either complementary or non-complementary ssDNA target. A theoretical detection limit of 1 nM is achieved in this work; an improvement of 74% in comparison to the previously reported work using a non-valved LOC (Ben-Yoav et al., 2012). This improvement is believed to be due to the increased experimental control and repeatability with the integrated microfluidic valved manipulation system and the amplified biosensing signal from diffusional reactions.

The LOC reported here can be scaled up to improve the repeatability of the test, as well as to enable a cost-effective, easy to operate, and low sample volume platform. Future work will be focused on testing the device with simulated and real-world samples (e.g., biological fluids, water samples, etc.) for specific applications (e.g., healthcare, environmental monitoring), and evaluating the dominant chemical and physical factors affecting its performance. That platform can be also used for an extensive study of micro-scale phenomena in miniaturized devices and their effect on the sensitivity, limit of detection, and selectivity. For example, studying the effect of the dimensions of the electrode and the microfluidic channel on diffusional reactions will help to evaluate cross-reactivity between adjacent sensors that will establish design and operation guidelines for LOC miniaturization. These guidelines will enable a new class of portable biosensing devices for analysis of DNA.

Acknowledgments

The authors would like to thank the Robert W. Deutsch Foundation for financial support. The authors also appreciate the support of the Maryland NanoCenter and its FabLab.

Appendix A. Supplementary material

Supplementary data associated with this article can be found in the online version at http://dx.doi.org/10.1016/j.bios.2014.09.069.

References

Analytical Methods Committee, 1987. Analyst 112, 199–204.
Andrieux, C.P., Hapiot, P., Saveant, J.M., 1990. Chem. Rev. 90 (5), 723–738.
Bard, A.J., Faulkner, L.R., 2001. Electrochemical Methods: Fundamentals and Applications, 2nd ed. John Wiley & Sons Inc., New York.
Beebe, D.J., Mensing, G.A., Walker, G.M., 2002. Annu. Rev. Biomed. Eng. 4 (1), 261–286.
Ben-Yoav, H., Dykstra, P.H., Bentley, W.E., Ghodssi, R., 2012. Biosens. Bioelectron 38 (1), 114–120.
Ben-Yoav, H., Freeman, A., Sternheim, M., Shacham-Diamand, Y., 2011. Electrochim. Acta 56 (23), 7780–7786.
Bhushan, B., 2010. Springer Handbook of Nanotechnology, 3rd ed. Springer.
Bisquert, J., Compte, A., 2001. J. Electroanal. Chem. 499 (1), 112–120.
Bonanni, A., del Valle, M., 2010. Anal. Chim. Acta 678, 7–17.
Chee, M., Yang, R., Hubbell, E., Berno, A., Huang, X.C., Stern, D., Winkler, J., Lockhart, D.J., Morris, M.S., Fodor, S.P.A., 1996. Science 25, 610–614.
Craighead, H., 2006. Nature 442 (7101), 387–393.
Dittrich, P.S., Manz, A., 2006. Nat. Rev. Drug Discov. 5 (3), 210–218.
Dukkipati, V.R., Pang, S.W., 2006. Nanotechnology, 162–165.
Dutse, S.W., Yusof, N.A., 2011. Sensors 11 (6), 5754–5768.
Dykstra, P.H., Roy, V., Byrd, C., Bentley, W.E., Ghodssi, R., 2011. Anal. Chem. 83 (15), 5920–5927.
Fang, T.H., Ramalingam, N., Xian-Dui, D., Ngin, T.S., Xianting, Z., Kuan, A.T.L., Huat, E. Y.P., Hai-Qing, G., 2009. Biosens. Bioelectron. 24, 2131–2136.
Gervais, T., Jensen, K.F., 2006. Chem. Eng. Sci. 61, 1102–1121.
Ghallab, Y.H., Badawy, W., 2010. Lab-on-a-Chip: Techniques, Circuits, and Biomedical Applications. Artech House.
Gooding, J.J., Chou, A., Mearns, F.J., Wong, E., Jericho, K.L., 2003. Chem. Commun. 15, 1938–1939.
Henry, O.Y.F., O'Sullivan, C.K., 2012. Trac – Trends Anal. Chem. 33, 9–22.
Hong, J., Edel, J.B., deMello, A.J., 2009. Drug Discov. Today 14, 134–146.
Ito, T., Hosokawa, K., Maeda, M., 2007. Biosens. Bioelectron 22 (8), 1816–1819.
Jiang, H., Weng, X.A., Li, D.Q., 2011. Microfluid. Nanofluid. 10 (5), 941–964.
Kim, J.H.-S., Marafie, A., Jia, X.-Y., Zoval, J.V., Madou, M.J., 2006. Sens. Actuator B – Chem. 113, 281–289.
Konopka, S.J., McDuffie, B., 1970. Anal. Chem. 42, 1741–1746.
Ma, K.-S., Zhou, H., Zoval, J., Madou, M., 2006. Sens. Actuator B – Chem. 114, 58–64.
Mariella, R., 2008. Biomed. Microdevices 10 (6), 777–784.
McEwen, G.D., Chen, F., Zhou, A., 2009. Anal. Chim. Acta 643, 26–37.
Nicholson, R.S., 1965. Anal. Chem. 37 (11), 1351–1355.
Pan, S., Rothberg, L., 2005. Langmuir 21 (3), 1022–1027.
Pavlovic, E., Lai, R.Y., Wu, T.T., Ferguson, B.S., Sun, R., Plaxco, K.W., Soh, H.T., 2008. Langmuir 24 (3), 1102–1107.
Ricci, F., Lai, R.Y., Heeger, A.J., Plaxco, K.W., Sumner, J.J., 2007. Langmuir 23 (12), 6827–6834.
Siegel, R., Ma, J., Zou, Z., Jemal, A., 2014. CA – Cancer J. Clin. 64 (1), 9–29.
Song, H., Ismagilov, R.F., 2003. J. Am. Chem. Soc. 125, 14613–14619.
Sun, Y., Kwok, Y.C., 2006. Anal. Chim. Acta 556, 80–96.
Tai, C.H., Ho, C.L., Chen, Y.L., Chen, W., Lee, G.B., 2013. Microfluid. Nanofluid. 15 (6), 745–752.
Xu, X., Zhang, S., Chen, H., Kong, J., 2009. Talanta 80, 8–18.
Xu, Y., Yang, X., Wang, E., 2010. Anal. Chim. Acta 683, 12–20.
Yang, A.H.J., Hsieh, K., Patterson, A.S., Ferguson, B.S., Eisenstein, M., Plaxco, K.W., Soh, H.T., 2014. Angew. Chem. 53 (12), 3163–3167.
Yang, W., Woolley, A.T., 2010. J. Lab. Autom. 15, 198–209.